Supplementary Information

Rapid chemically selective 3D imaging in the mid-infrared with a Si-based camera

Eric O. Potma[1,2,*,**], David Knez[1], Yong Chen[3], Amanda Durkin[2], Alexander Fast[2], Mihaela Balu[2], Brenna Norton-Baker[1], Rachel W. Martin[1], Tommaso Baldacchini[1,#], Dmitry A. Fishman[1,*,**]

[1] *Department of Chemistry, University of California Irvine, 92697 CA, United States*
[2] *Beckman Laser Institute, University of California Irvine, 92697 CA, United States*
[3] *Epstein Department of Industrial and Systems Engineering, Los Angeles, CA 90089, United States*
[4] *Department of Molecular Biology & Biochemistry, University of California Irvine, 92697 CA, United States*
[#] *currently with Edwards Life Sciences, Irvine, 92612 CA, United States*

* these authors contributed equally
** dmitryf@uci.edu
epotma@uci.edu

Supplementary Table 1. Experimental parameters.

MIR pulse width	~110 fs
MIR power	1.5 mW @ 1 kHz (not accounted for camera window absorption)
NIR power	0.15 mW @ 1 kHz
MIR spot size	3.5 mm
NIR spot size	4 mm
Pixel size	6.5 mm x 6.5 mm
CCD active area	1392x1040 pixels
CCD protective window	Fused silica 1.5 mm
Estimated quantum efficiency for MIR only*	$1*10^{-9}$

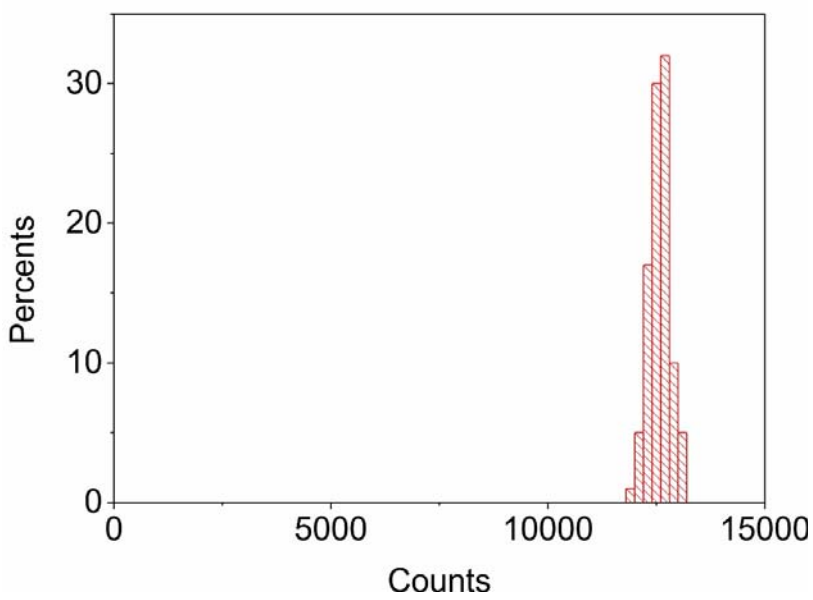

Supplementary Figure SF1. Beam intensity stability for a single pixel at the center of the beam at 2850 cm^{-1}. Standard deviation σ=0.019 measured for 100 s integration time with 0.1 s frame rate.

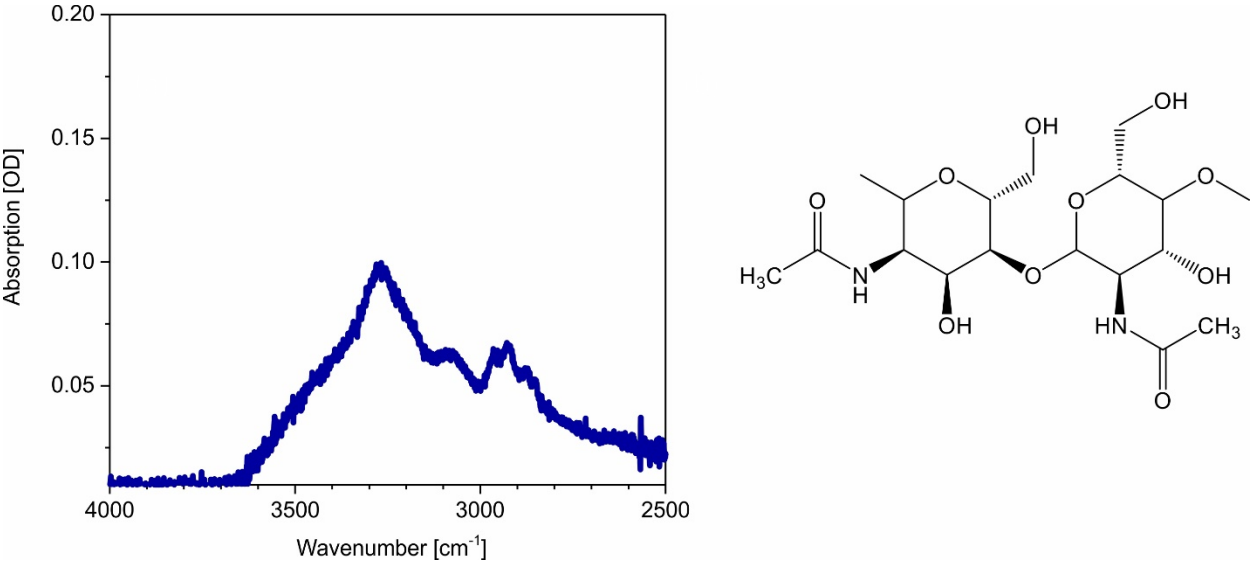

Supplementary Figure SF2. FTIR-ATR spectrum of chitin (bee wing).

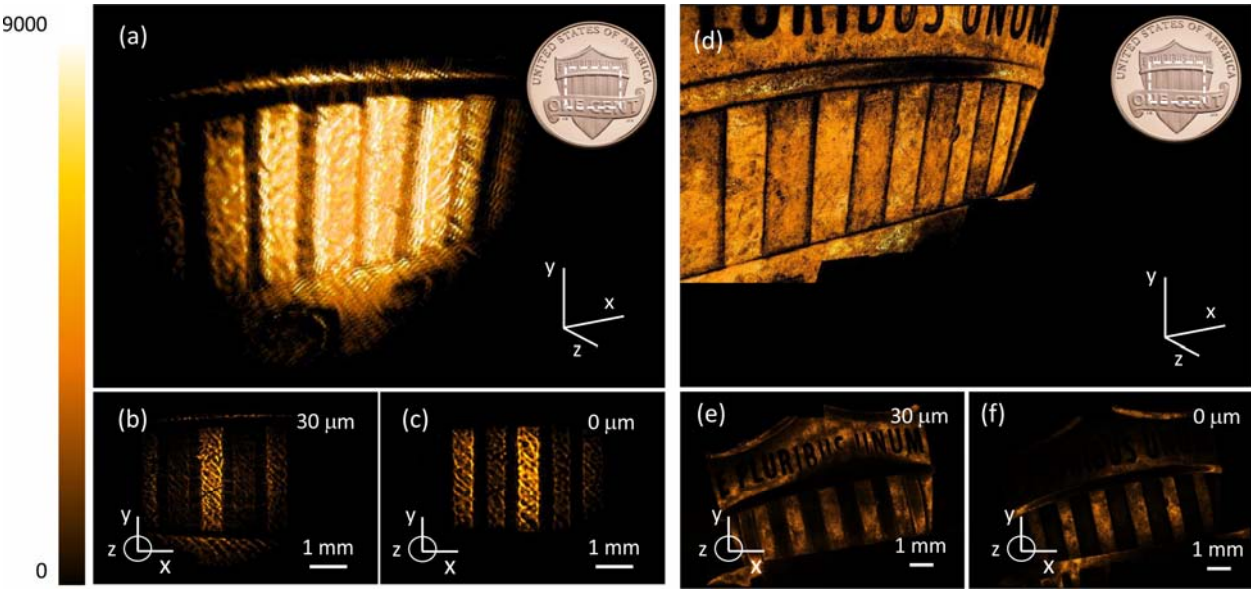

Supplementary Figure SF3. (a, b, c) Tomographic imaging of the structured metal surface of a one cent US coin (Union Shield). (a) 3D reconstruction, (b) and (c) are frames measured at height h=30 µm and h=0 µm, respectively. (d) 3D reconstruction of confocal reflection imaging of the coin. (e) and (f) are 2D confocal scans measured at height difference 30 µm.

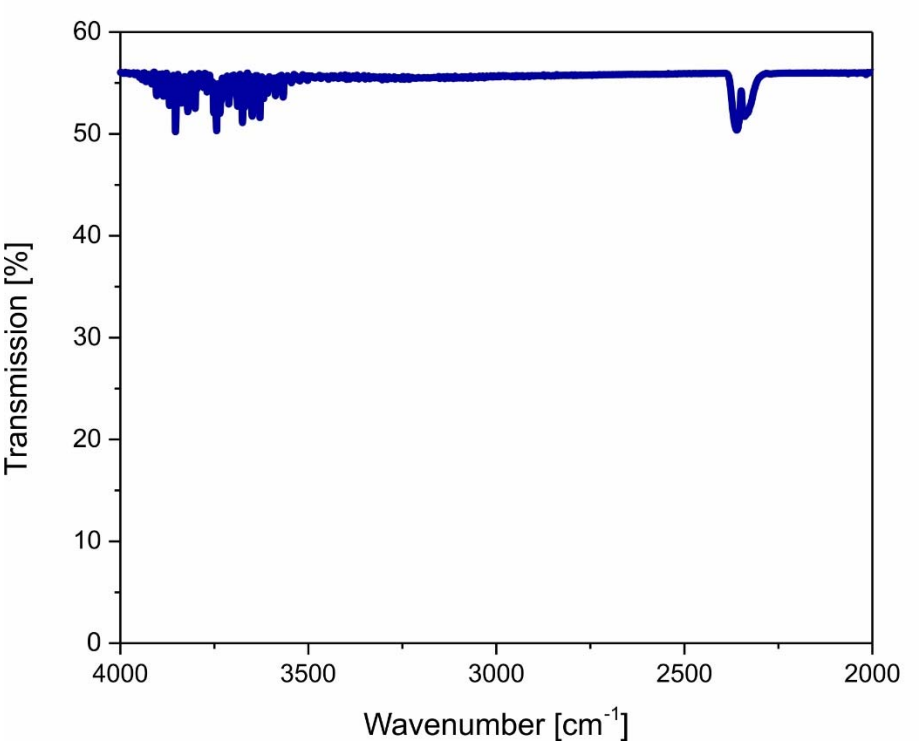

Supplementary Figure SF4. FTIR transmission spectrum of a 3 mm GaAs wafer. Main IR light loss attributed to Fresnel reflection at the semiconductor/air interfaces. In double path, this results in ~25% transmission.

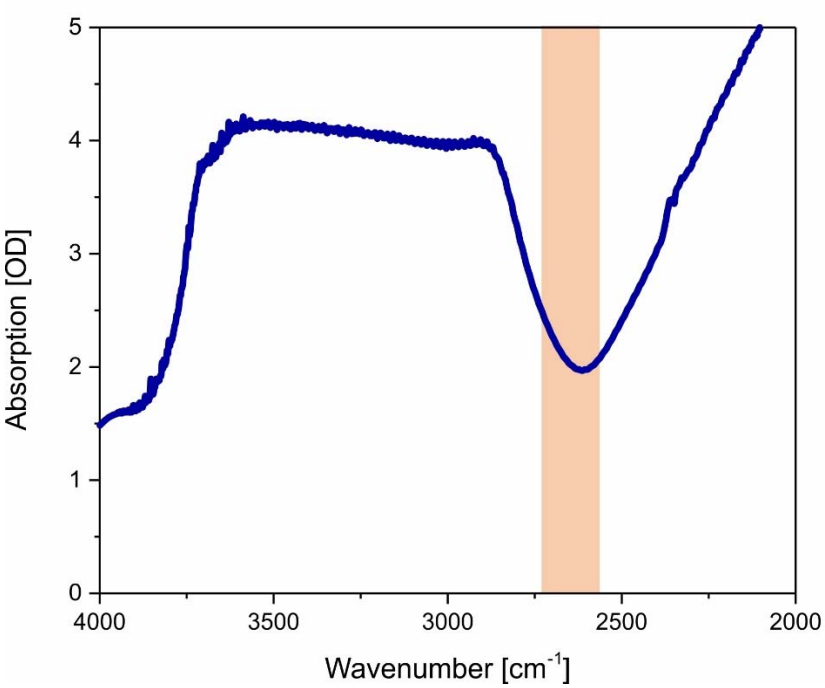

Supplementary Figure SF5. FTIR transmission spectrum of a 380 μm water layer. Rectangle represents pulse spectral bandwidth.

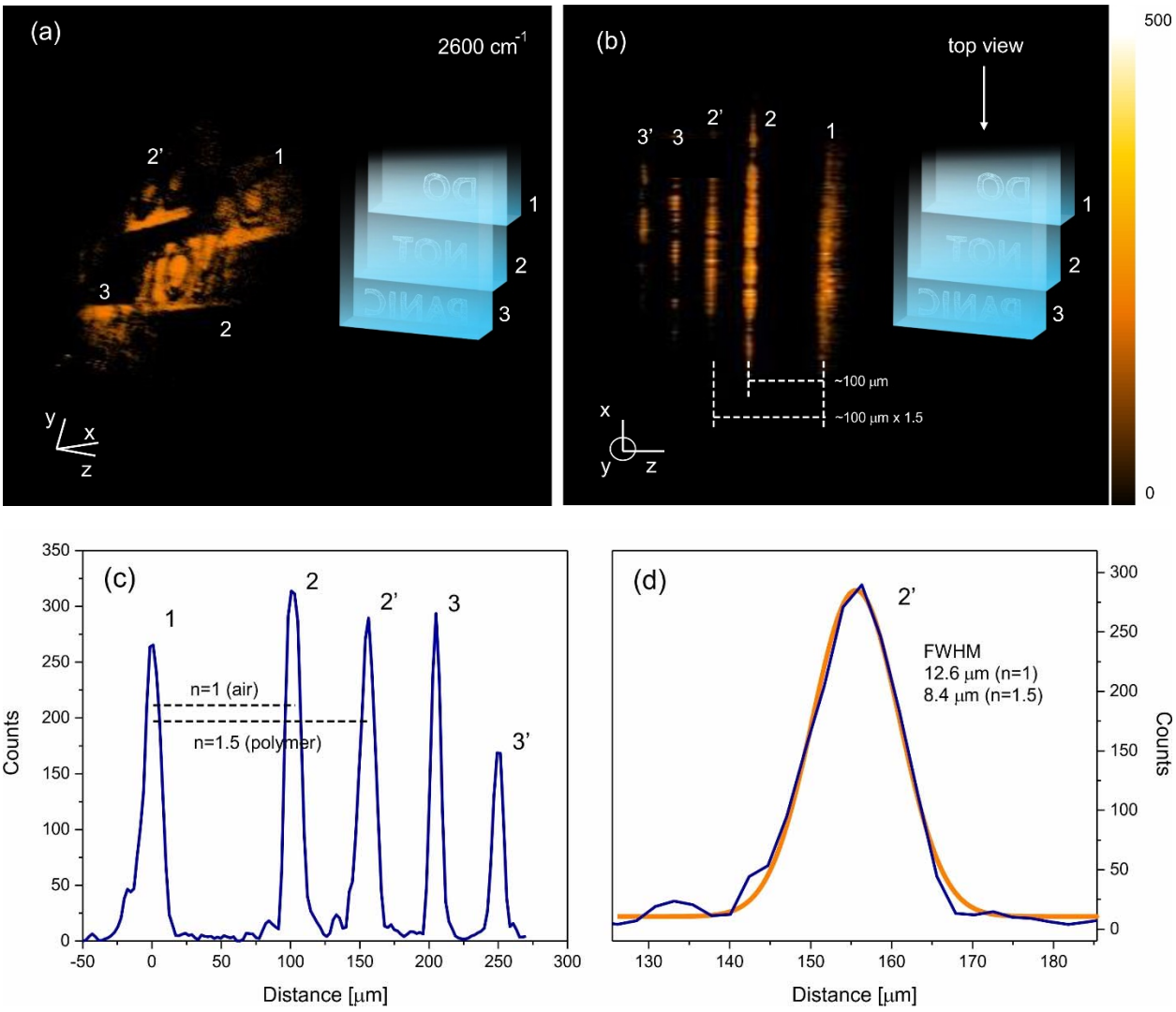

Supplementary Figure SF6. 3D imaging of cellulose acetate transparency ladder at 2600 cm^{-1} shown at different perspective angles (a) and (b). Though reflected from the same surface 2, photons propagating through cellulose acetate sheet 1 are temporally delayed (2') with respect to photons that travel in air (2). (c) Spatial cross-section of MIR pulse propagation in layered cellulose acetate structure. (d) Gauss fit for response on 2' interface (propagation through cellulose acetate). FWHM indicates spatial resolution of 12.6 μm.

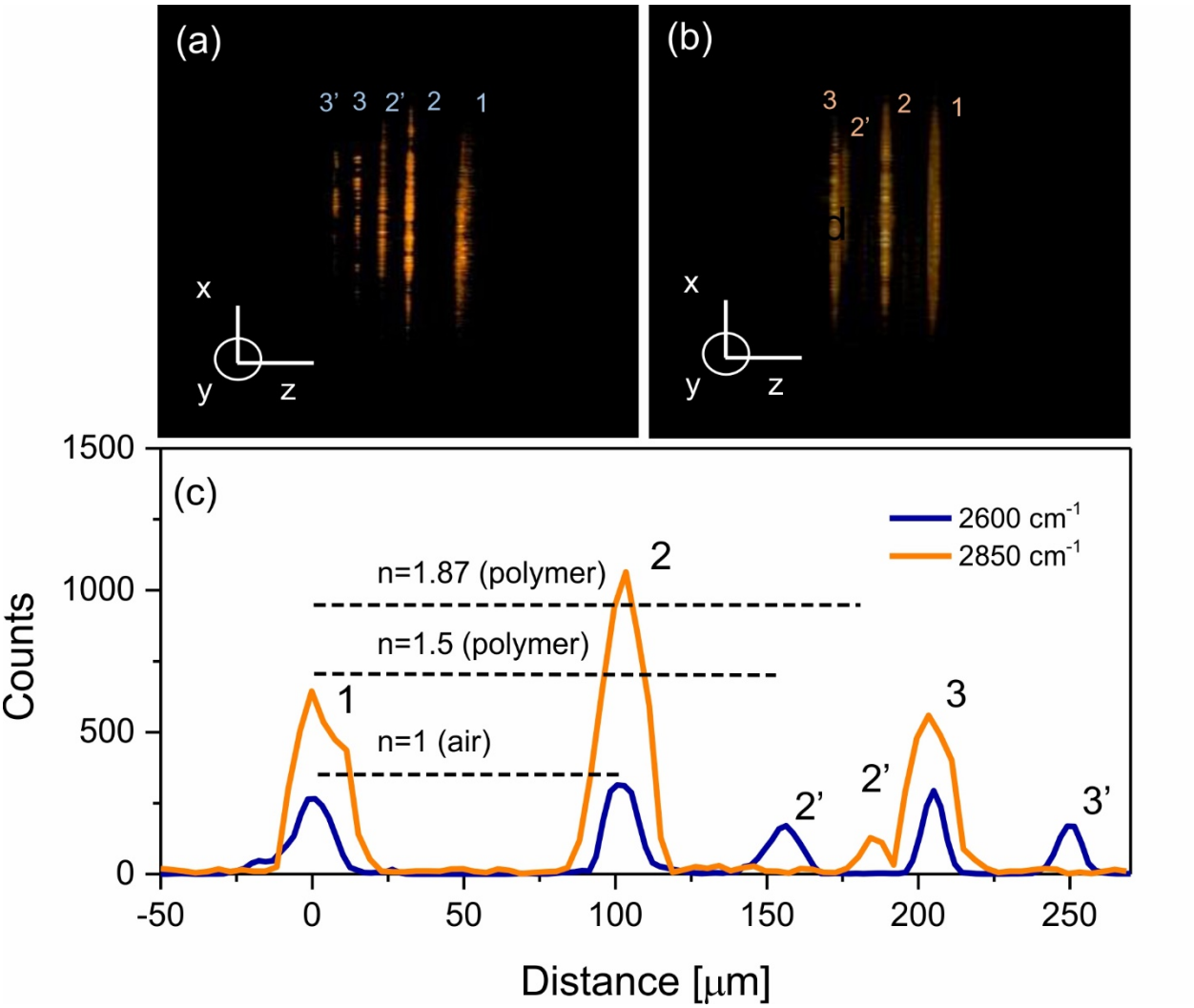

Supplementary Figure SF7. 3D image of cellulose acetate structure imaged at 2600 cm^{-1} and 2850 cm^{-1} for top view perspective similar to Figure SF5b. (c) Peak positions of reflections off the different interfaces. The difference between the peak positions found for propagation in air and polymer reveals that n~1.5 for 2600 cm^{-1} and n~1.87 for 2850 cm^{-1}.

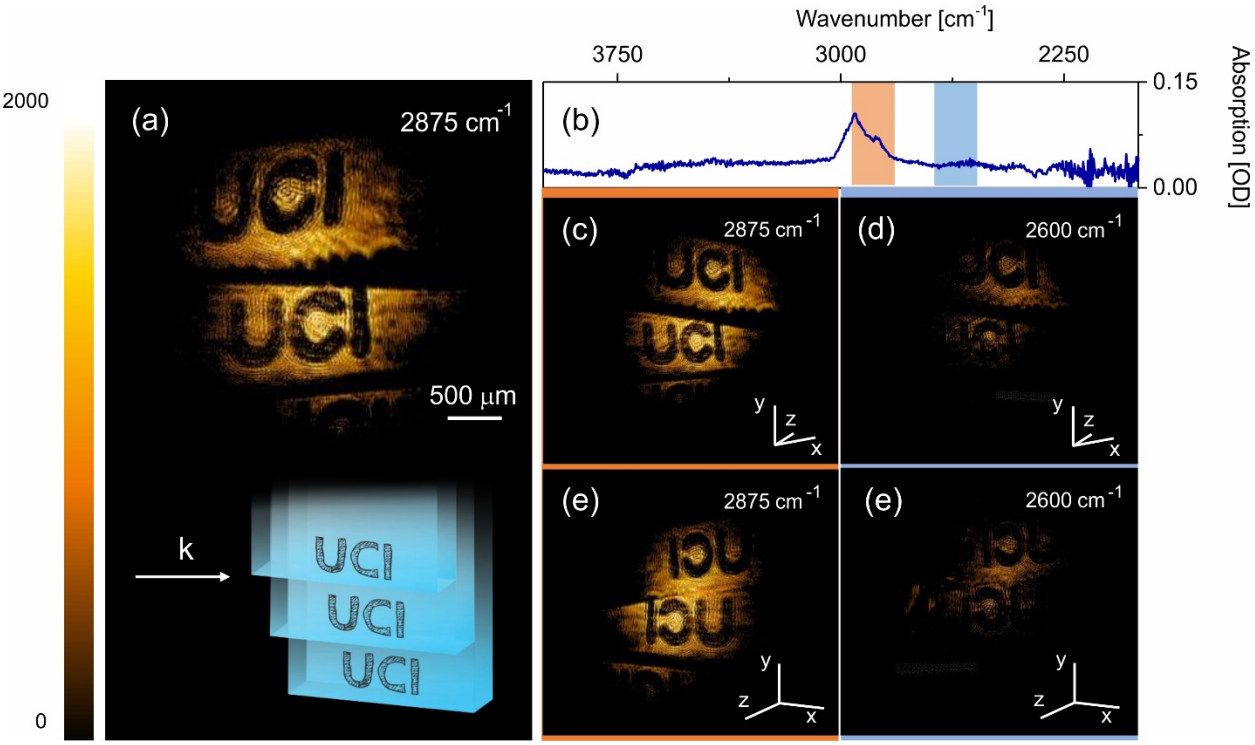

Supplementary Figure SF8. 3D imaging of cellulose acetate transparency ladder. (a) 3D reconstruction of transparency ladder with printed letters. (b) FTIR transmission spectrum of cellulose acetate sheet. Rectangles represent Gaussian pulse width of ~150 cm^{-1}. (c) and (e) 3D imaging at 2850 cm^{-1}, (d) and (e) 3D imaging at 2600 cm^{-1}. Total 3D image acquisition time is 1s.

Supplementary Figure SF9. Optical image of designed resin structure.

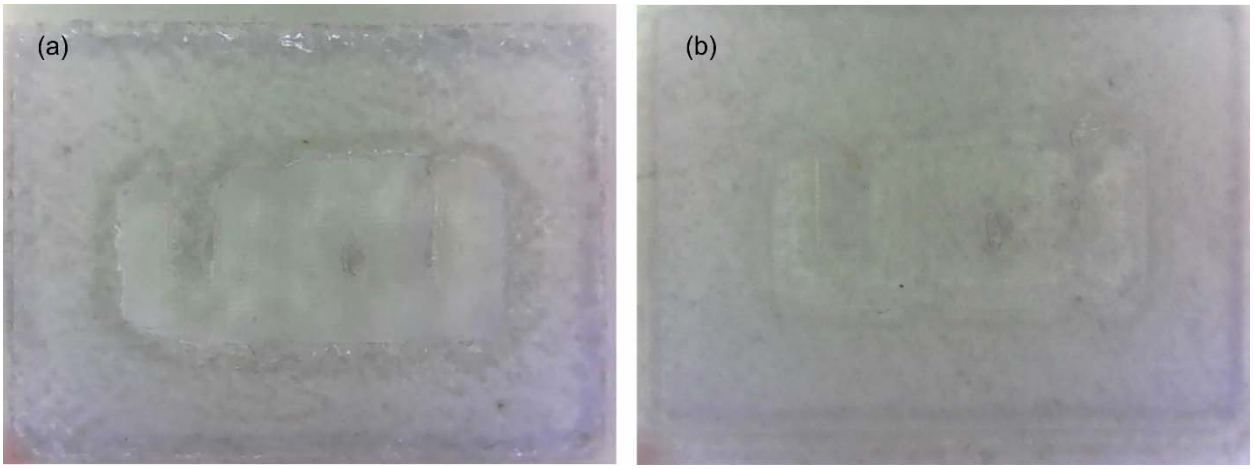

Supplementary Figure SF10. Optical imaging of designed resin structure clean (b) and embedded in silicone lubricant (a).

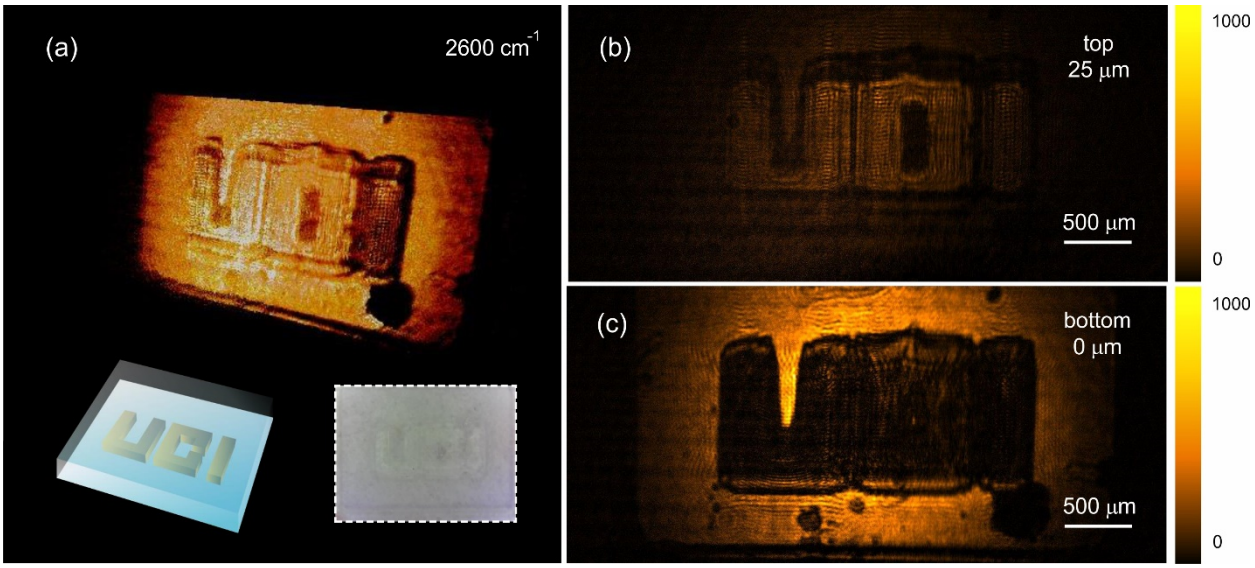

Supplementary Figure SF11. Imaging of designed resin structure embedded in silicone lubricant. (a) Full 3D scan (Inset: 3D rendering and optical image), (b) cross section at height (b) 25 μm and (c) 0 μm. Total 3D scan 0.5 seconds.

The structures presented in Supplementary Figures SF8 and SF9 were manufactured with the approach outlined in the Methods section of the main text. This particular structure has several fabrication defects and clear differences between the polymerized layers (Supplementary Figure SF9a). If embedded in silicone lubricant, a compound with a strong MIR absorption around 2900 cm^{-1}, it becomes barely visible to the eye due to refractive index matching (Supplementary Figure SF8b). However, the structure is clearly resolved in IR, using our 3D imaging approach (Supplementary Figure SF9) with good contrast if tuned on and off the 2900 cm^{-1} absorption resonance of the silicone lubricant (Supplementary Figure SF10).

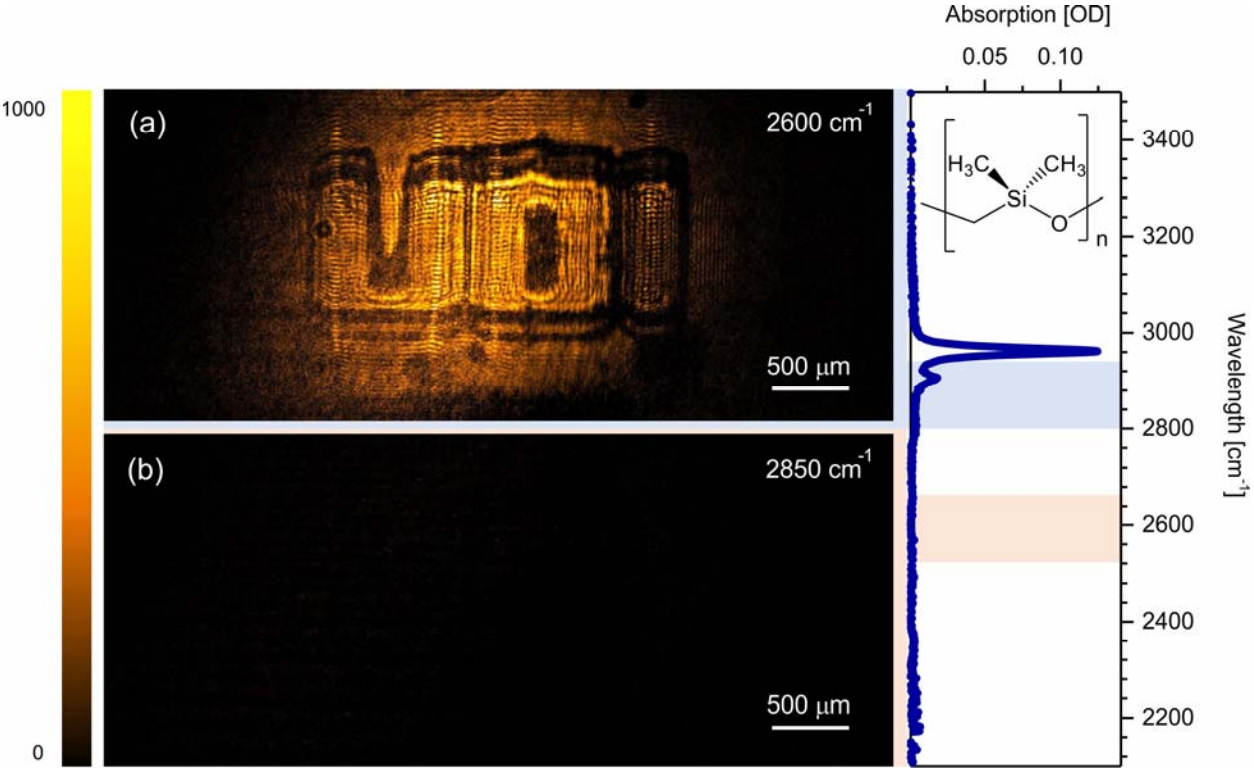

Supplementary Figure SF12. 3D imaging of resin structure embedded in silicone lubricant. (a) 2600 cm^{-1}, (b) 2850 cm^{-1}. Spectrum shows the MIR absorption of the silicone lubricant.

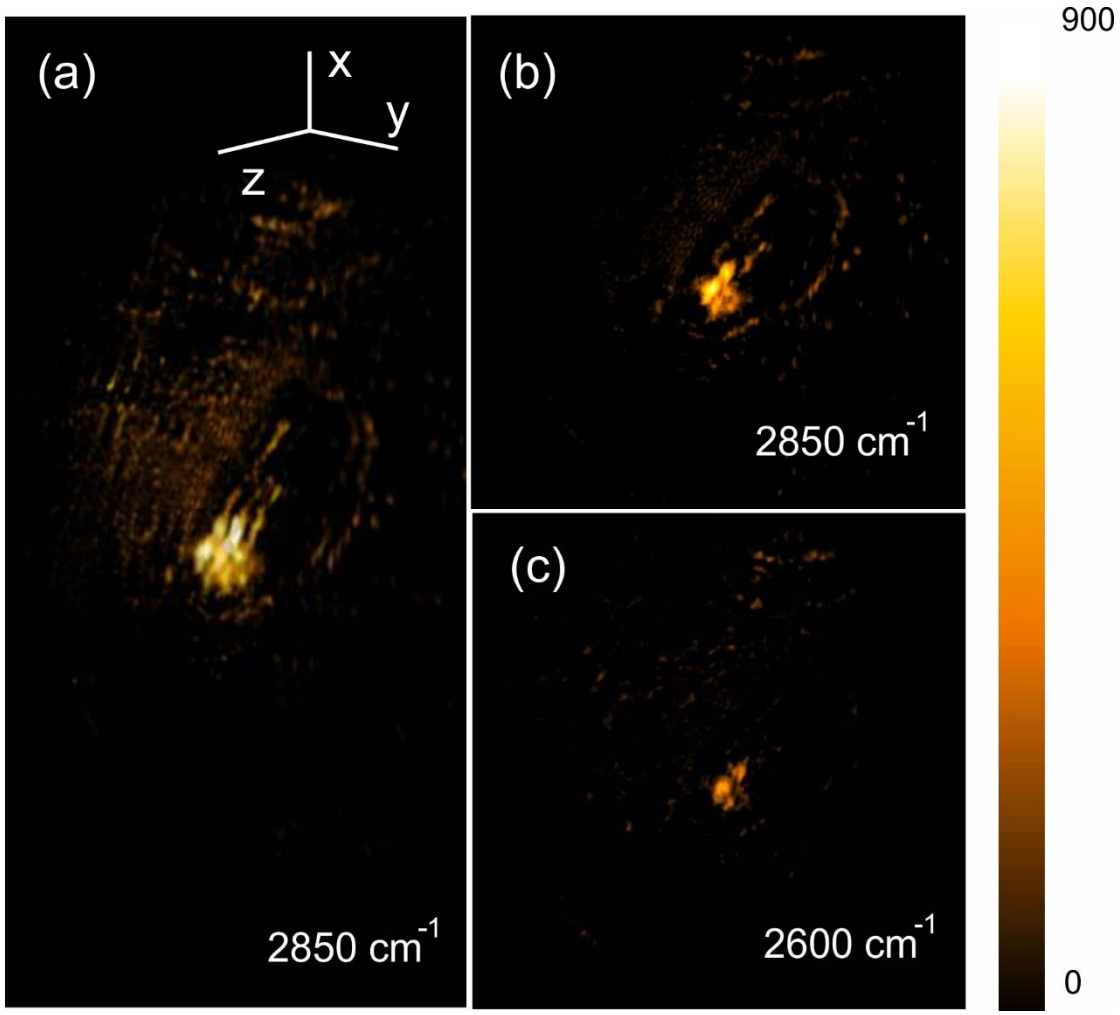

Supplementary Figure SF13. Imaging of lysozyme crystals on mica glass. (a) 3D reconstructions at 2850 cm^{-1}. 2D image of crystal top at 2850 cm^{-1} (b) and (c) 2600 cm^{-1}.